catalysts

MDPI

Review

Photocatalytic CO_2 Conversion to Ethanol: A Concise Review

Dezheng Li †, Chunnan Hao †, Huimin Liu *, Ruiqi Zhang, Yuqiao Li, Jiawen Guo, Clesio Calebe Vilancuo and Jiapeng Guo

School of Chemical and Environmental Engineering, Liaoning University of Technology, Jinzhou 121001, China
* Correspondence: liuhuimin08@tsinghua.org.cn
† These authors contributed equally to this work.

Abstract: Photo-catalytically converting the greenhouse gas CO_2 into ethanol is an important avenue for the mitigation of climate issues and the utilization of renewable energies. Catalysts play critical roles in the reaction of photocatalytic CO_2 conversion to ethanol, and a number of catalysts have been investigated, including semiconductors and plasmonic metal-based catalysts, as well as several other catalysts. In this review, the progress in the development of each category of catalysts is summarized, the current status is reviewed, the remaining challenges are pointed out, and the future research directions are prospected, with the aim being to pave pathways for the rational design of better catalysts.

Keywords: photocatalysis; CO_2 conversion; ethanol; semiconductor; plasmonic metal

Citation: Li, D.; Hao, C.; Liu, H.; Zhang, R.; Li, Y.; Guo, J.; Vilancuo, C.C.; Guo, J. Photocatalytic CO_2 Conversion to Ethanol: A Concise Review. *Catalysts* **2022**, *12*, 1549. https://doi.org/10.3390/catal12121549

Academic Editor: Jose L. Hueso

Received: 28 October 2022
Accepted: 29 November 2022
Published: 1 December 2022

1. Introduction

With the proposal of the concept of "emission peaking" and "carbon neutralization", the conversion and utilization of CO_2 have been put on the agenda [1–5]. Photo-catalytically converting CO_2 into valuable fuels is a promising approach, since it could mitigate the climate issues caused by greenhouse gas CO_2 and store the renewable solar energy as chemical energy simultaneously [6–9]. The products of CO_2 photocatalytic conversion reactions include CO [10–12], CH_4 [13,14], CH_3OH [15,16], C_2H_5OH [17–20], HCOOH [21,22], etc. Noteworthily, C_2H_5OH (ethanol) is a chemical with wide applications in the chemical industry, medical and healthcare industries, food industry, agriculture production, and so on. Therefore, photocatalytic CO_2 conversion to ethanol has recently become a research hotspot.

Catalysts play an essential role in the reaction of photocatalytic CO_2 conversion to ethanol. Up to now, a great number of photocatalysts have been developed, such as TiO_2 [23], Bi_2MoO_6 [24], g-C_3N_4 [25], Cu/TiO_2 [26], and AuCu/g-C_3N_4 [27]. Based on the nature of the developed catalysts, they could roughly be divided into semiconductors, plasmonic metal-based catalysts, and several others (Scheme 1).

Up to the present, there have been many excellent reviews on CO_2 photocatalytic reactions. However, some of them focused on a special type of catalyst, such as a semiconductor [28,29] or Mexene [30], while some of them focused on the conversion of CO_2 to CH_4 [31] or other products [32]. To the best of our knowledge, there have been no reviews on catalysts for photocatalytic CO_2 reduction to ethanol. In this paper, the progress of each category of catalysts (Scheme 1) for photocatalytic CO_2 conversion to ethanol is summarized, and the current research status and the future prospect are reviewed, with the aim being to give the readers a clear picture and to inspire more studies to further advance this research area.

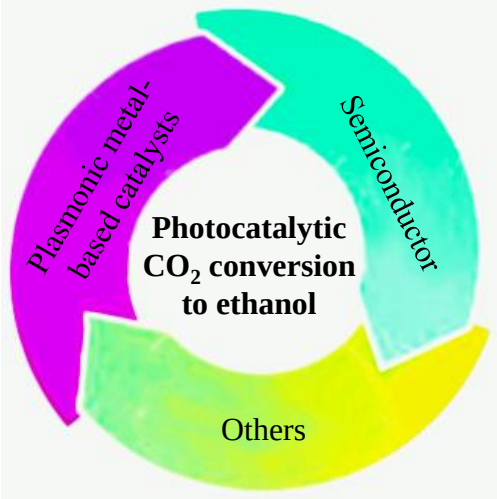

Scheme 1. Schematic illustration of the catalysts used for photocatalytic CO_2 conversion to ethanol.

2. Semiconductor Based Catalysts

Semiconductors describe a category of materials which can harness solar light. Upon the irradiation of solar light with photon energy, $h\nu$ matches or exceeds the bandgap energy of the semiconductor, and an electron jumps from the valence band (VB) to the conduction band (CB), leaving a hole. The electrons and holes can combine and dissipate the input energy as heat or transfer it to the catalyst surface. In the case that the position of CB is lower than the potential required for CO_2 conversion to ethanol, the electron reacts with the adsorbed species and participates in a CO_2 reduction reaction to produce ethanol (Figure 1). According to this principle, several semiconductors have been verified to be active in photocatalytic CO_2 conversion to ethanol.

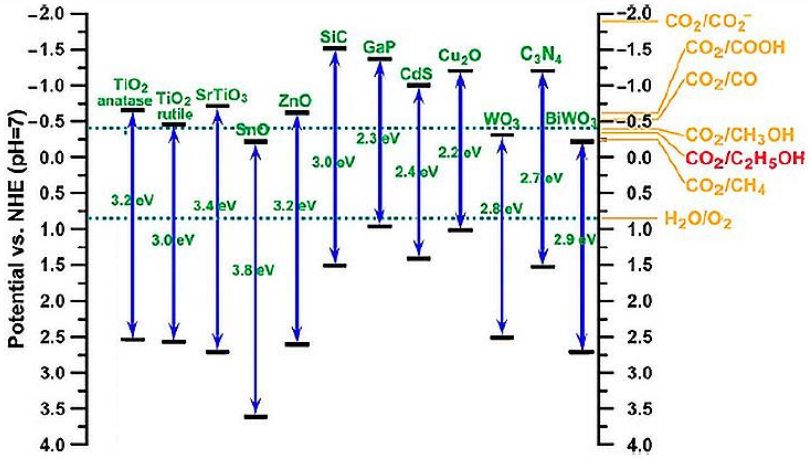

Figure 1. Band structure of several typical semiconductors with respect to CO_2 reduction potentials towards different products at pH = 7. Reproduced with permission from reference [33].

There are several factors affecting the efficiency of photocatalytic CO_2 conversion to ethanol, as follows: (1) Light absorption region and efficiency. Solar light mainly consists of a large amount of infrared light, visible light, and a small amount of ultraviolet light. Absorbing more light means more energy can be utilized to promote the reaction. The bandgap of the catalysts is an important factor influencing the light absorption region. Meanwhile, the energy levels of the catalysts should meet the requirement of the reaction. Therefore, upon suitable energy levels, the bandgap width of the catalysts should be as small as possible to absorb more sunlight to improve the photocatalytic activity and conversion efficiency. (2) The separation and transfer of photogenerated electron–hole

pairs. As catalysis is a surface reaction process, photogenerated electrons and holes must be separated and transferred to the surface to react with the adsorbates. However, photogenerated electron–hole pairs are unstable and easy to recombine during transfer. Therefore, facilitating the electron–hole pairs' separation and transfer is effective for accelerating the reaction. (3) Photogenerated electrons and holes react with the surface adsorbates, respectively, to give products. Not all the photogenerated electrons and holes can react with the adsorbates. ① The positions of the conduction band and valence band must correspond to the positions of the corresponding reaction levels in order to have sufficient redox capacity. ② For different reactants, their ability to adsorb electrons and holes is also different. In order to ensure the smooth progress of the surface reaction, it is usually required that the reactants have sufficient adsorption on the catalyst surface, and can receive the electrons and holes on the surface smoothly.

2.1. Pristine Semiconductors

Pristine semiconductors, such as TiO_2, Bi_2MoO_6, BiOCl, and TaON, have been reported to be active in photocatalytic CO_2 conversion to ethanol. For instance, self-organized TiO_2 nanotube arrays could serve as a photocatalyst for the conversion of CO_2 to alcohols under xenon lamp irradiation, with the methanol and ethanol formation rates are ~10.0 nmol cm^{-2} h^{-1} and ~9.0 nmol cm^{-2} h^{-1}, respectively [23]. The large specific surface area and the one-dimensional nanotubular structure of TiO_2 nanotube arrays accounted for catalytic activities (Figure 2a). The mechanism is proposed as follows (Figure 2b). Upon light irradiation, electrons and holes are generated over TiO_2 nanotube arrays. The holes react with adsorbed H_2O to form hydroxyl radicals and hydrogen ions. The interaction between hydrogen ions and the excited electrons leads to hydrogen radicals. Meanwhile, the photoexcited electrons transfer to the conduction band and react with CO_2 to produce $\cdot CO_2^-$. However, $\cdot CO_2^-$ is not stable and will be transformed to chemisorbed ·CO, which is subsequently reduced to $\cdot CH_2$ and eventually yields methanol and ethylidene by reaction with ·OH and ·H. Ethanol is formed via the reaction of ethylidene, ·OH, and ·H (Figure 2b).

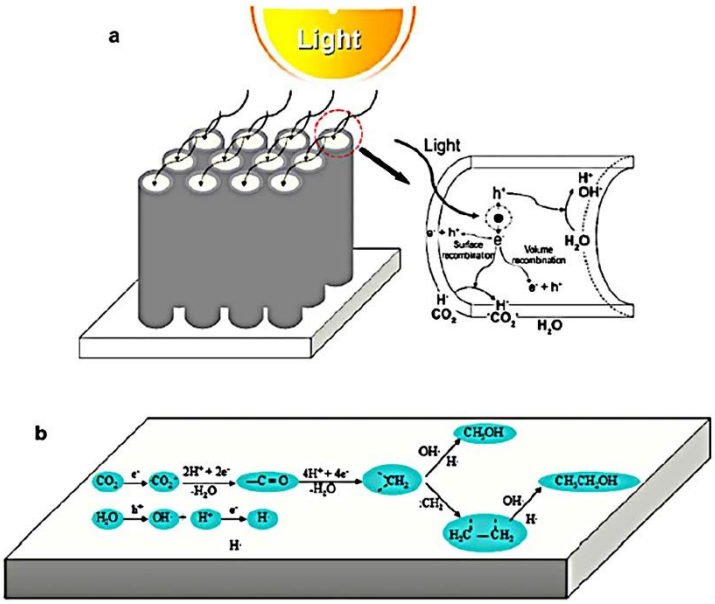

Figure 2. (**a**) Schematic illustration of the photocatalytic CO_2 reduction to alcohols over TiO_2 nanotubes, and (**b**) proposed mechanism of photocatalytic CO_2 reduction to methanol and ethanol over TiO_2 nanotubes. Reproduced with permission from reference [23].

Furthermore, Bi_2MoO_6 is another pristine semiconductor for photocatalytic CO_2 conversion to ethanol. Dai et al. reported that hierarchical flower-like Bi_2MoO_6 exhibited high catalytic activity for the photocatalytic reduction of CO_2 under visible light irradiation, with

methanol and ethanol yields of 6.2 and 4.7 μmol g^{-1} h^{-1}, respectively [34]. Ribeiro et al. fabricated Bi_2MoO_6 catalysts by a simple hydrothermal or solvothermal method and investigated the effects of synthesis parameters on their performance in CO_2 photoreduction in an aqueous medium under visible light irradiation, with the aim to pave pathways for the rational design of better catalysts in the future [35]. It was discovered that the pH value of the precursor suspensions was a key factor in determining the properties (such as zeta potential, crystallinity, and morphology) and performance of Bi_2MoO_6 catalysts. The more acidic the pH values, the higher ethanol production rates. The Bi_2MoO_6 synthesized with H_2O as the solvent and pH = 2 gave the highest ethanol yield, reaching 34.4 μmol g^{-1} h^{-1} [35].

Several other Bi-based pristine semiconductors, such as $BiVO_4$ [36], Bi_2WO_6 [24], and BiOCl [37], have also been successfully applied in photocatalytic CO_2 reduction to ethanol. Taking $BiVO_4$ as an example, Huang et al. reported that a large number of C_1 intermediates could be generated on the surface of $BiVO_4$ under highly intensive light irradiation, which dimerized to produce ethanol [36]. Monoclinic $BiVO_4$ was more efficient than tetragonal $BiVO_4$ for ethanol production, recording an ethanol production rate of 2033.0 μmol g^{-1} h^{-1} under a 300 W Xe-arc lamp irradiation, without the detection of methanol as a byproduct [36].

Additionally, TaON [38] and $SrZrO_3$ [39] are also promising in photocatalytic CO_2 reduction to ethanol. Here, $SrZrO_3$ is taken as a representative example for elaboration. He et al. prepared $SrZrO_3$ nanoparticles via a sonochemical method and employed it in a photocatalytic CO_2 reduction reaction [39]. Ethanol, methane, and carbon monoxide were detected as the main products, with an ethanol production rate of 10.2 μmol g^{-1} h^{-1} under the irradiation of a 300 W xenon lamp. Characterization results suggested that the position of CB of $SrZrO_3$ was 1.37 eV vs. vacuum and −3.13 eV vs. NHE, which lies above the redox potential of methane, ethanol, and carbon monoxide, indicating all of them are possible products of CO_2 reduction by $SrZrO_3$. Upon light irradiation, electron–hole pairs were generated. The electrons activated CO_2 on the catalyst surface to form $\cdot CO^{2-}$ and reacted with H^+ in the solution to produce ·H. The interaction between $\cdot CO^{2-}$ and ·H gave CO. The resultant CO could also be converted into ·C, followed by the formation of ·CH, $\cdot CH_2$, and $\cdot CH_3$ through successive reactions, which then reacted with H_2O, H^+ or OH to produce ethanol or methane [39].

In spite of the fact that several pristine semiconductors have been successfully applied in the reaction of photocatalytic CO_2 reduction to ethanol, their efficiencies are generally low, due to their weak light absorption capacity, low photon utilization efficiency, and so on [40,41]. In this regard, several approaches have been adopted to modify the semiconductors, for example, by delicately introducing vacancy sites and constructing a heterojunction or hybrid catalyst with another semiconductor or non-semiconductor material, with the aim being to further improve their catalytic performance. In the following several sub-sections, we will review the progress of modified semiconductors in photocatalytic CO_2 reduction to ethanol.

2.2. Semiconductors with Vacancy Sites

Delicately introducing vacancy sites into semiconductors is an important approach to extend the light absorption spectrum, narrow the bandgap, and regulate the electronic structure of pristine semiconductors. Semiconductors with vacancy sites have also been studied in photocatalytic CO_2 reduction to ethanol.

Yang et al.'s work is a typical example [42]. They synthesized a Bi_2MoO_6 catalyst by assembling two-dimensional ultra-thin Bi_2MoO_6 nanoflakes into three-dimensional nanospherical Bi_2MoO_6. During the assemble process, abundant oxygen vacancies were created, resulting in two primary sites, namely the oxygen vacancies and the exposed molybdenum atoms (Figure 3). The two primary sites served as dual binding sites to trap CO_2 for its activation into electronic CO* species, which were subject to accepting electrons and holes, realizing the selective reduction of CO_2 into methanol and ethanol. Under

visible light irradiation, the as-prepared Bi_2MoO_6 catalyst afforded methanol and ethanol production rates of 26.6 μmol g^{-1} h^{-1} and 2.6 μmol g^{-1} h^{-1}, respectively, far surpassing those of bulk Bi_2MoO_6 [42].

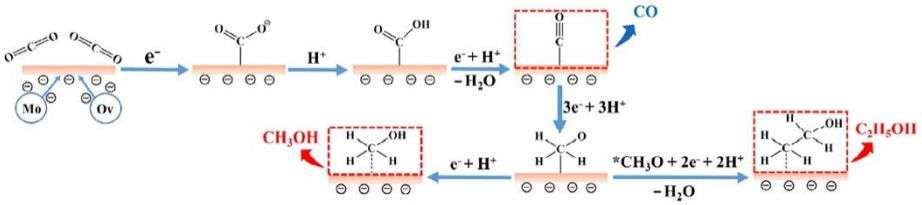

Figure 3. Proposed reaction pathway of photocatalytic CO_2 reduction to methanol and ethanol. Reproduced with permission from reference [42].

Do et al.'s work is another example that falls into this category [43]. The authors reduced a $HCa_2Ta_3O_{10}$ nanosheet and used it as a catalyst for photocatalytic CO_2 reduction with H_2O. It was discovered that the reduction process induced a considerable amount of Ta^{4+} and oxygen vacancies, which significantly improved the visible light harvesting capacity of $HCa_2Ta_3O_{10}$ [43]. Introducing CuO onto reduced $HCa_2Ta_3O_{10}$ further enhanced its performance in photocatalytic CO_2 reduction to alcohols, with ethanol and methanol production rates of 113.0 μmol g^{-1} h^{-1} and 7.4 μmol g^{-1} h^{-1}, respectively. The enhanced performance was ascribed to the facilitated separation of photogenerated electron–hole pairs due to the formation of p–n junctions as well as the boosted CO_2 adsorption and stabilization of C_1 intermediates by CuO [43].

2.3. Heterojunctions

Heterojunctions constructed by two or more semiconductors generally exhibit stronger light absorption capacity and a narrower bandgap than their corresponding single semiconductor counterparts. A number of heterojunctions have been adopted as catalysts for photocatalytic CO_2 reduction to ethanol, including g-C_3N_4/ZnTe [44], Cu_2O/g-C_3N_4 [45], Co_3O_4/CeO_2 [46], MoS_2/Bi_2WO_6 [47], TiO_2/$Ni(OH)_2$ [48], Bi/Bi_2MoO_6 [49], TiO_2/Ti_3C_2 [50], CuO/TiO_2 [51], and AgBr/TiO_2 [52].

Here, the applications of TiO_2/Ti_3C_2 [50] and P25 (heterojunction between anatase and rutile TiO_2) [53] in photocatalytic CO_2 reduction to ethanol are chosen as representatives for elaboration. The TiO_2/Ti_3C_2, synthesized by a facile hydrothermal oxidation method, exhibited a narrowed band gap and enhanced light harvesting capacity [50]. The ratio between TiO_2 and Ti_3C_2 affected the optical properties and performance of the heterojunctions. After the functionalization by imine ligands and Pd nanoparticles, the performance of the catalysts in CO_2 activation and water splitting was further promoted. The TiO_2/Ti_3C_2 with an optimal TiO_2:Ti_3C_2 ratio recorded an ethanol production rate of ~10.0 μmol cm^{-2} h^{-1} at −0.6 V [50]. In case that P25 was used as a photocatalyst for CO_2 conversion with H_2O, multiple products, including O_2, H_2, C_1-C_4 hydrocarbons, methanol, ethanol, and acetone were detected, with an ethanol yield of 0.14 μmol g^{-1} h^{-1}, under the illumination of a 100 W UV-LED in a wavelength range of 355–385 nm and a light intensity of 120 mW cm^{-2} [53]. The specific structure and the intensive light illumination accounted for the high ethanol yield over P25 [53].

A Z-scheme is a special category that falls into the class of heterojunctions. Catalysts with a Z-scheme structure have also been investigated in photocatalytic CO_2 reduction to ethanol. For instance, Seeharaj et al. constructed TiO_2/rGO/CeO_2 (rGO is reduced graphene oxide) catalysts by combining surface-modified TiO_2 nanoparticles with rGO and CeO_2 [54]. The TiO_2 surface was initially modified via the sono-assisted exfoliation method in 10 M NaOH for 1 h, which led to increased specific surface area, enhanced light absorption, and a decreased recombination rate of photoinduced electron–hole pairs. The incorporation of rGO and CeO_2 further boosted the separation and transfer of photogenerated charges, electron mobility, and CO_2 absorptivity. The high interfacial contact area and strong interaction between modified TiO_2, rGO, and CeO_2 resulted in a high photocatalytic

CO_2 reduction rate, with methanol and ethanol production rates of 641.0 μmol g^{-1} h^{-1} and 271.0 μmol g^{-1} h^{-1}, respectively [54]. The reaction mechanism is proposed with a schematic illustration in Figure 4. The photocatalytic CO_2 reduction reaction is a two-step process, involving water splitting and CO_2 photoreduction. Upon light irradiation, both modified TiO_2 and CeO_2 were excited, forming electrons in CB and holes in VB. Then, the holes from the modified TiO_2 VB transferred to CeO_2 VB and subsequently oxidized H_2O into OH·, H^+, and O_2. Meanwhile, the electrons at CeO_2 CB transferred to modified TiO_2 CB and then to the rGO sheet. The multiple electrons were collected and transported along the rGO sheet to reduce the adsorbed CO_2 to form intermediates, such as $\cdot CO_2$ and ·CO. Eventually $\cdot CO_2$ and ·CO reacted with H^+ to obtain methanol and ethanol [54].

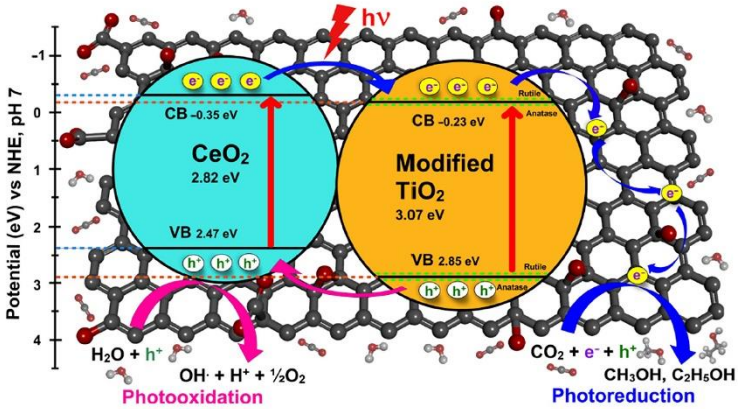

Figure 4. Proposed mechanism for photocatalytic CO_2 reduction to methanol and ethanol over a TiO_2/rGO/CeO_2 catalyst. Reproduced with permission from reference [54].

2.4. Hybrid Catalysts Constructed between a Semiconductor and a Non-Semiconductor Material

Fabricating a hybrid catalyst by combining a semiconductor with a non-semiconductor material is another avenue to tailor the physicochemical and optical properties of semiconductors. Quantum dots (QD), metal organic frameworks (MOFs), conducting materials, and isolators have been adopted as modifiers to construct this type of hybrid catalyst.

(1) QD–semiconductor hybrid catalysts. The QDs are nanoparticles of semiconductors and describe a category of nanoscale crystals that can transport electrons [55,56]. In this regard, QD–semiconductor hybrid catalysts generally exhibit extraordinary properties and performance. A number of QD–semiconductor hybrid catalysts have been constructed and applied in photocatalytic CO_2 reduction to ethanol, such as WS_2 QD/Bi_2S_3 [57], and Bi_2MoO_6 QD/rGO [58]. Taking WS_2 QD/Bi_2S_3 as an example, WS_2 QD/Bi_2S_3 constructed by decorating WS_2 QD onto Bi_2S_3 nanotubes by seed-mediated strategy was sensitive to visible/near-infrared light and displayed an excellent CO_2 photoreduction activity, with methanol and ethanol production rates of 9.6 μmol g^{-1} h^{-1} and 7.0 μmol g^{-1} h^{-1}, respectively [57]. Characterization results revealed that in WS_2 QD/Bi_2S_3, the exposed S atoms in WS_2 QD coordinated to Bi^{3+} to form a Bi–S bond, enabling the sharing of S atoms between WS_2 QD and Bi_2S_3 (Figure 5). The junction interface between WS_2 QD and Bi_2S_3 facilitated the separation and transfer of electron–hole pairs and consequently accounted for its enhanced catalytic performance [57]. Cheng et al.'s study is another example [59]. They prepared a CdS-Cu^{2+}/TiO_2 nanorod array film photocatalyst, in which a TiO_2 nanorod array was synthesized by a hydrothermal method, and CdS and Cu^{2+} were deposited on TiO_2 by a cation adsorption method and successive ion layer adsorption reaction (SILAR). Its performance in photocatalytic reduction of CO_2 under visible light irradiation was measured under visible-near infrared light. The results showed that the yield of ethanol reached the maximum value (109.1 μmol g-cat^{-1} h^{-1}) when SILAR was deposited twice, at a flow rate of 4 mL min^{-1} and a reaction temperature of 80 °C. The high catalytic activity of CdS-Cu^{2+}/TiO_2 was attributed to the combination of one-dimensional

nanostructure with Cu^{2+} ions and CdS quantum dots, which restrained the recombination of the electron–hole pairs and broadened the visible light responsive region [59].

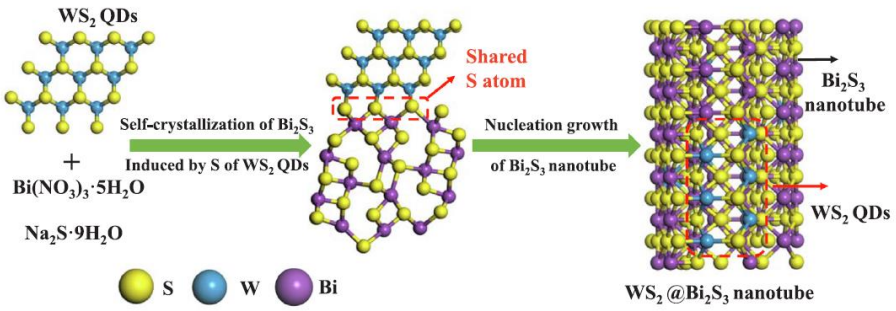

Figure 5. Schematic illustration of the structure of WS_2 QD/Bi_2S_3. Reproduced with permission from reference [57].

(2) The MOF–semiconductor hybrid catalysts. The MOFs are a class of porous polymeric materials, in which metal ions are linked together by organic bridging ligands. These MOFs usually have the advantages of highly porous structure, large specific surface area, and adjustable pore size, which endow them special properties as modifiers or catalysts [60–62]. For instance, Liu et al. encapsulated CuO QDs in the pores of MIL-125(Ti) (MIL-125(Ti) is a type of MOF) and further combined it with g-C_3N_4 to fabricate a g-C_3N_4/CuO@MIL-125(Ti) catalyst, which exhibited a high catalytic activity for photocatalytic CO_2 reduction in the presence of H_2O, with yields of CO, methanol, acetaldehyde, and ethanol up to 60.0 μmol g^{-1} h^{-1}, 332.4 μmol g^{-1} h^{-1}, 177.2 μmol g^{-1} h^{-1}, and 501.9 μmol g^{-1} h^{-1}, respectively [63]. A mechanism study revealed that, under light irradiation, electrons and holes were generated and separated (Figure 6). Due to the positions of the energy levels of g-C_3N_4, CuO QDs, and MIL-125(Ti), the electrons remained at CB of CuO QDs, and the holes remained at VB of g-C_3N_4. The potential energy of electrons on CB of CuO QDs met the requirements for CO_2 reduction to CO, methanol, acetaldehyde, and ethanol, and led to the generation of these products. The valence band of g-C_3N_4 was more positive than the oxidation potential of H_2O, resulting in the oxidation of H_2O to O_2 [63]. Cardoso et al. prepared a hybrid catalyst via growing MOF-based nanoparticles (ZIF-8) on Ti/TiO_2 nanotubes and adopted the as-prepared Ti/TiO_2-ZIF-8 catalyst in the photocatalytic CO_2 reduction reaction. The Ti/TiO_2-ZIF-8 can produce ethanol up to 10.0 mmol L^{-1}. The increased photocurrent (ZIF-8 acted as a cocatalyst to interact with Ti/TiO_2 nanotubes) and promoted electron transfer accelerated CO_2 photocatalytic reduction to ethanol [64].

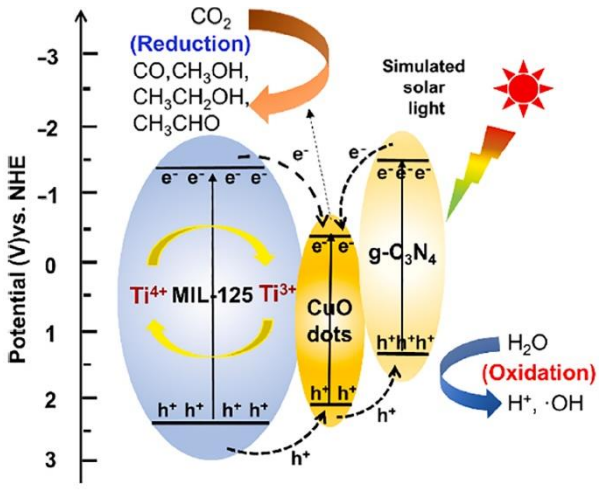

Figure 6. Schematic illustration of photoexcited electron–hole separation process over g-C_3N_4/CuO@MIL-125(Ti). Reproduced with permission from reference [63].

(3) Conducting material–semiconductor hybrid catalysts. Integrating a semiconductor with a conducting material is an avenue to facilitate the electron transfer and prohibit the recombination of photoexcited electron–hole pairs [65,66]. For instance, modifying semiconductor Bi_2WO_6 with conducting polymers tailored the photoelectronic properties (band gap, charge mobility, etc.) and promoted the photocatalytic performance in photocatalytic CO_2 reduction [65]. Under visible light irradiation, the as-fabricated catalyst demonstrated methanol and ethanol yields of 14.1 μmol g^{-1} h^{-1} and 5.1 μmol g^{-1} h^{-1}, respectively [65]. Similarly, graphitic-supported multiple functionalized TiO_2 nanowire (denoted as R-TiO_2@Gs) recorded an ethanol yield of 124.2 μM in CO_2 reduction with water after light irradiation for 6 h. The graphitic support accelerated the electron transfer, while the ligands in functionalized TiO_2 enabled the catalyst to capture CO_2 more efficiently and facilitated C–C coupling to produce ethanol [67].

(4) Isolator–semiconductor hybrid catalysts. Loading a semiconductor onto an isolator with a large specific surface area could increase the number of active sites and enhance the photocatalytic activity. Du and co-author's work is representative of this [68]. They constructed a TPS/g-C_3N_4 (TPS is trimodal porous silica) composite catalyst via a two-step hydrothermal synthesis method. The TPS/g-C_3N_4 catalysts were of hollow tubular shapes, with a large specific surface area, high CO_2 adsorption capacity, and more active sites. Consequently, TPS/g-C_3N_4 exhibited a high activity in photocatalytic CO_2 reduction reaction to ethanol, with an ethanol yield of 196.0 μmol g^{-1} h^{-1} and an ethanol selectivity of ~100% [68].

2.5. Doped Semiconductors

Doped semiconductors generally exhibit engineered energy levels and bandgaps, which improve the light absorption and facilitate the separation and transfer of electron–hole pairs.

For example, Maimaitizi et al. prepared hollow-graded BiOCl microspheres co-doped with N and Pt by an in situ hydrothermal method and explored its performance in CO_2 photoreduction to ethanol [69]. Under visible light irradiation, the ethanol yield reached 14.15 μmol $g_{cat}{}^{-1}$ h^{-1}. Results suggested that the scattering effect and surface reflection caused by the special layered structure of the catalyst, the narrowing of the bandgap caused by N doping, and the Schottky barrier caused by the existence of Pt accelerated the charge separation and transfer, and consequently accounted for the high catalytic performance [69]. Li et al. successfully synthesized a Zn-doped g-C_3N_4 catalyst by a one-step calcination method and investigated the effects of operational conditions on its performance in CO_2 photoreduction under ultraviolet or visible light irradiation [70]. Notably, the optimized 0.5%Ru/Zn-g-C_3N_4-1/20 catalyst gave the best photocatalytic activity, with the yield of ethanol reaching 1442.9 μmol g^{-1}. A mechanism study revealed that electrons were transferred to Ru through Zn–N bonds and reacted with adsorbed CO_2 during light irradiation. At the same time, CH_4 combined with holes to form methyl, which can be attracted by Ru and connects with *CHO to form acetaldehyde intermediate. When some of the intermediates were converted to acetaldehyde, most of them were further hydrogenated to form ethanol [70].

3. Plasmonic Metal-Based Catalysts

Plasmonic metals, such as Cu, Ag, Au, and their alloys, are sensitive to visible light and could act as active sites for photocatalytic reactions [71,72]. Plasmonic metal-based catalysts have also been widely applied in photocatalytic CO_2 reduction to ethanol [73,74]. Generally speaking, plasmonic metal-based catalysts give higher activities than semiconductors for CO_2 photoreduction. In this section, the progress of plasmonic metals-based catalysts for the photocatalytic conversion of CO_2 to ethanol is reviewed.

3.1. Cu-Based Catalysts

(1) Cu nanoparticle-based catalysts. These Cu nanoparticles are of plasmonic properties and have been studied in photocatalytic CO_2 reduction to ethanol. For example, Xuan et al. took the advantages of the plasmonic effect of Cu and the chemical absorption capacity of CO_2 by Cu@Ni to fabricate a $SrTiO_3$/Cu@Ni/TiN catalyst [75]. The as-prepared $SrTiO_3$/Cu@Ni/TiN could capture full-spectrum solar energy and activate CO_2 efficiently, and consequently exhibited an ethanol evolution rate of 21.3 μmol g^{-1} h^{-1} and an ethanol selectivity of 79% under the irradiation of a 600 mW cm^{-2} Xe lamp [75]. Density functional theory calculation suggested that CO_2 activation was the rate-determining step and that CO_2* was easier to absorb on the interface of Cu (100) and Ni (111) (Figure 7). In addition, CO* was difficult to desorb at the interface of Cu (100) and Ni (111), which facilitated the dimerization of CO to produce ethanol (Figure 7) [75]. Similarly, Cu-TiO_2/GO (GO = graphene oxide) synthesized via a one-step hydrothermal method was effective for photocatalytic CO_2 reduction to ethanol, with an ethanol production rate of 233 μmol g^{-1} h^{-1} [76]. The high specific surface area, the narrowed band gap, and the plasmonic properties of Cu accounted for its performance [76].

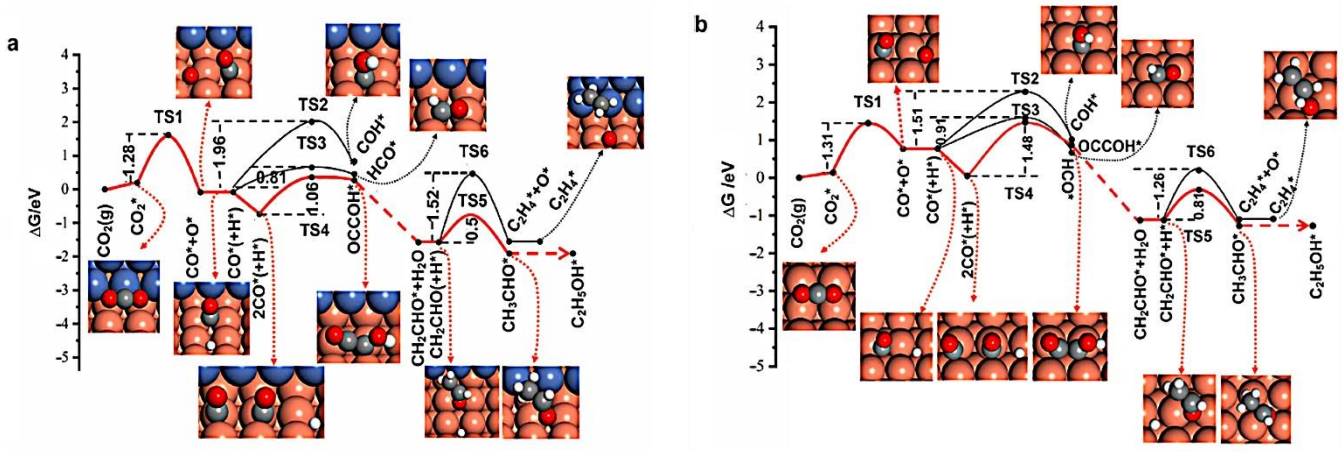

Figure 7. (**a**) Free energy diagram for CO_2 reduction to ethanol and ethylene on the Cu@Ni interface, (**b**) free energy diagram for CO_2 reduction to ethanol and ethylene on Cu (100) surface. The red line represents the lowest energy path. The Cu, Ni, C, O, and H atoms are shown in brown, blue, gray, red, and white, respectively. Reproduced with permission from reference [75].

(2) Cu ion-based catalysts. Here, Cu^I could selectively catalyze CO_2 conversion to ethanol; however, the catalytic sites of Cu^I are not stable. Incorporating Cu^I into the cavities of MOFs or decorating Cu single atoms onto MOFs could retain the chemical state of Cu^I [77,78]. In this regard, several light responsive Cu–MOFs catalysts have been designed for photocatalytic CO_2 reduction to ethanol. For instance, Lin et al. used low intensity light to activate an in situ $Cu^{II}(H_xPO_4)_y$@Ru-Uio catalyst to generate Cu^I species in the cavities of Uio-67 [77]. Upon light irradiation, one single electron transferred from photoexcited $[Ru(bpy)_3]^{2+}$-based ligands on Uio-67 to Cu^{II} centers in the cavities and one single hole transferred from Cu^0 to $[Ru(bpy)_3]^{2+}$-based ligands for the generation of Cu^I (Figure 8). The Cu^I then served as the active centers for photocatalytic CO_2 reduction to ethanol, with an activity of 9650.0 μmol $g_{Cu}{}^{-1}$ h^{-1} at 150 °C [77].

The Cu^{2+} incorporated into semiconductors can also serve as a catalyst to drive the reaction of photocatalytic CO_2 reduction to ethanol, such as Cu doped into TiO_2 [26,79]. The preparation method, as well as the morphology of TiO_2, strongly affected the properties and performance of the as-prepared Cu-TiO_2 catalysts. The Cu-doped TiO_2 nanorod, which was synthesized via the combination of the hydrothermal method and ultrasonic assisted sequential adsorption method, exhibited improved photon transfer due to the one-dimensional nanostructure of TiO_2 and the incorporation of Cu^{2+}, and resulted in methanol and ethanol yields of 36.2 μmol g^{-1} h^{-1} and 79.1 μmol g^{-1} h^{-1} at 80 °C and UV

light irradiation [26]. The Cu-TiO_2 nanocatalyst fabricated by the sol-gel method possessed a large specific surface area, increased number of oxygen vacancies, and enhanced atomic mobility, which improved CO_2 photoreduction by H_2O, with methane, hydrogen, methanol, ethanol, and acetaldehyde as products [79].

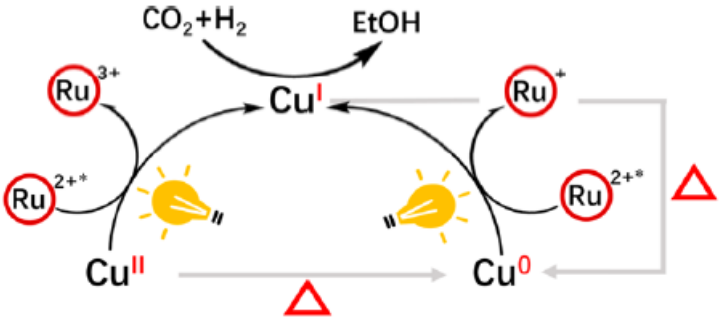

Figure 8. Generation of Cu^I via light irradiation over a $Cu^{II}(H_xPO_4)_y$@Ru-Uio catalyst (* represents the active site). Reproduced with permission from reference [77].

(3) CuO semiconductor-based catalyst. In recent years, CuO has attracted extensive attention in the field of photocatalytic CO_2 reduction due to its strong absorption capacity towards solar energy. In addition, the combination of CuO with other semiconductors could reduce the rapid recombination of photogenerated electron–hole pairs and produce ethanol under light irradiation. For example, Lu et al. prepared a Re-doped CuO/TiO_2-NTs catalyst by doping rhenium into CuO/TiO_2 nanotube arrays, which gave methanol and ethanol as the main products in photocatalytic CO_2 reduction reaction. With the increase in Re, the proportion of ethanol in the product increased (Figure 9), with the optimized yield of ethanol reaching 7.5 µmol over 6wt% re-doped CuO/TiO_2-NTs after applying an external voltage of 0.4 V under simulated solar light illumination. The remarkable result might have originated from the tuned interface characteristics of re-doped CuO/TiO_2-NTs, which promoted the selectivity towards alcohols and accelerated the occurrence of the C–C coupling reaction [80].

3.2. Ag-Based Catalysts

Another plasmonic metal, Ag, has been utilized in photocatalytic CO_2 reduction to ethanol. For example, Shu et al. synthesized an Ag@AgBr/carbon nanotubes (CNT) nanocomposite catalyst by anchoring Ag@AgBr nanoparticles onto the surface of CNT, and investigated the effects of CNT length on the performance of Ag@AgBr/CNT in photocatalytic CO_2 reduction reaction under visible light irradiation [81]. It was discovered that CNT with longer length facilitated the separation of electron–hole pairs. Together with the plasmonic properties of Ag and the unique structure of Ag@AgBr/CNT nanocomposite, Ag@AgBr/CNT with longer CNT length exhibited a promoted activity in CO_2 reduction to methane, CO, methanol, and ethanol, with an ethanol yield of ~5.0 µmol g^{-1} h^{-1} [81]. This was not only limited to Ag@AgBr/CNT, as Ag@AgBr/AgCl also showed activity for CO_2 conversion to methanol and ethanol under visible light irradiation [82].

3.3. Au-Based Catalysts

The Au-based catalysts are another type of plasmonic metal for CO_2 reduction to ethanol. Do et al. deposited plasmonic Au nanoparticles onto ZIF-67 (ZIF-67 is a type of MOF) and investigated the performance of Au/ZIF-67 in a photocatalytic CO_2 reduction [83]. It was found that the loading of Au affected the size of Au nanoparticles, and Au nanoparticles with sizes in the range of 30–40 nm exhibited improved light harvesting capacity, enhanced charge separation, and played crucial roles in determining selectivity. Volcano relationships were obtained between the production rates of methanol/ethanol and the loading of Au, with an optimal ethanol production rate of 0.5 mmol g^{-1} h^{-1} (Figure 10a,b) [83]. The mechanism was proposed as follows: under light irradiation, plas-

monic Au were excited and generated energetic electrons. These electrons overcame the Schottky barrier and injected into ZIF-67, which then participated in the activation and conversion of CO_2 to methanol and ethanol, which had already been adsorbed on the surface of ZIF-67 (Figure 10c) [83]. Ramis et al. probed the key intermediates and products over Au/TiO_2 in a photocatalytic CO_2 reduction reaction [84]. They revealed that several different CO_2 adsorption modes (i.e., CO_2, bicarbonate, and carbonate) could be observed depending on the loading of Au. The presence of H_2O promoted the formation of CO_2 radicals. Methanol mainly adsorbed over TiO_2 sites, forming methoxy-species, which could be converted into ethanol [84]. The probation of the intermediates and products provided insights for the mechanism study.

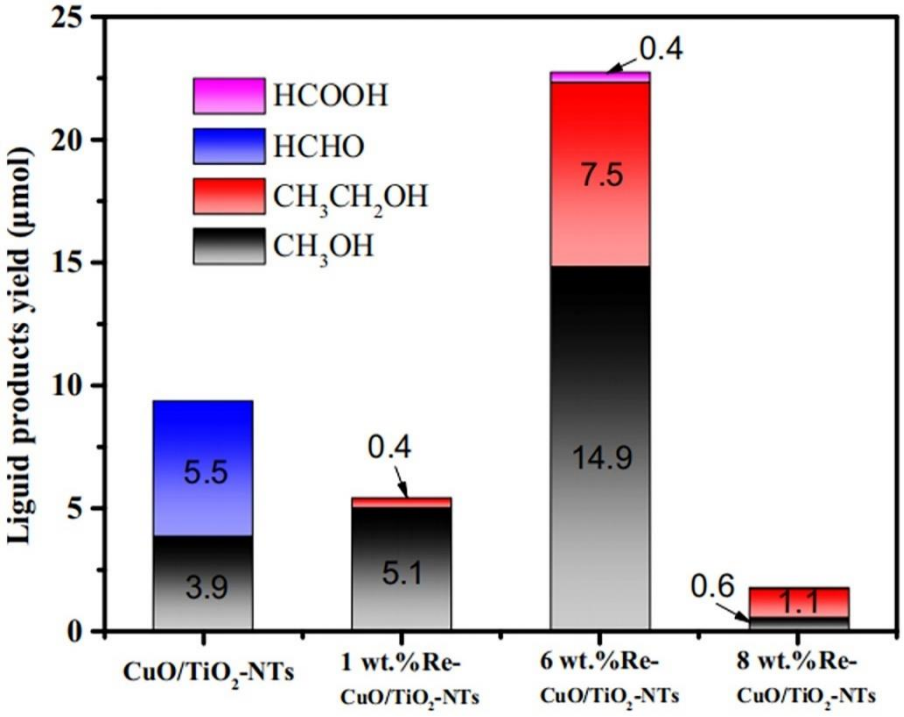

Figure 9. Yields of products over different de-doped CuO/TiO_2-NTs. Reproduced with permission from reference [80].

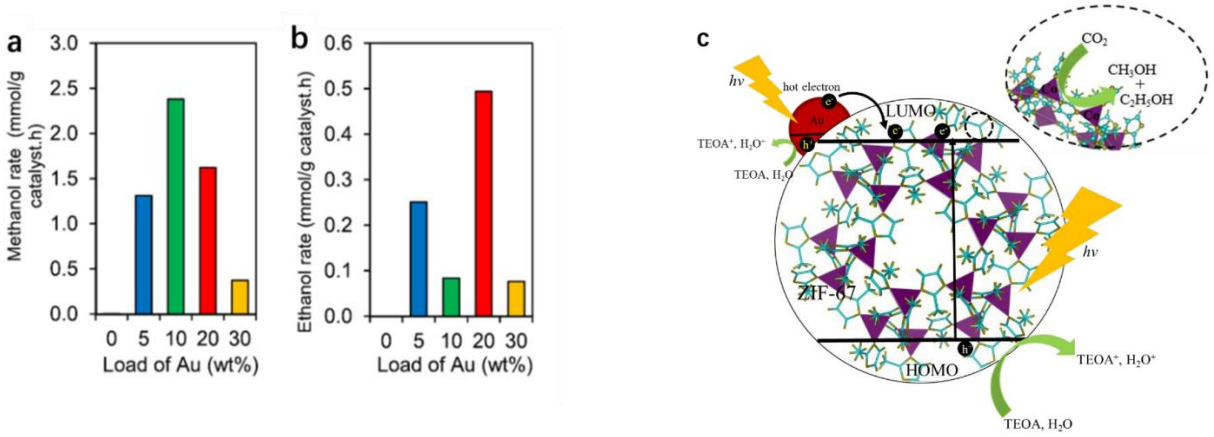

Figure 10. (**a**,**b**) Effects of loading of Au on the photocatalytic activity of Au/ZIF-67 in a photocatalytic CO_2 reduction. (**c**) Proposed mechanism for photocatalytic CO_2 reduction to methanol and ethanol over Au/ZIF-67. Reproduced with permission from reference [83].

3.4. Plasmonic Alloy-Based Catalysts

Plasmonic alloys exhibit not only the plasmonic properties but also some specific properties [11], which empower their applicability in photocatalytic CO_2 reduction to ethanol. For instance, AuCu/g-C_3N_4 was a very promising catalyst, affording an ethanol yield and selectivity of 0.9 mmol g^{-1} h^{-1} and 93.1%, respectively [27]. In addition to the plasmonic properties, the alloy structure of AuCu, as well as the interactions between AuCu and g-C_3N_4, contributed to its photocatalytic performance. Over AuCu alloy, Au was positively charged, and Cu was negatively charged due to their electronegativity difference. The positive charge on Au promoted CO_2 adsorption and the negative charge on Cu facilitated the formation of the intermediates $CO_2{\cdot}^-$ and *CO. The interaction between AuCu and g-C_3N_4 facilitated the transfer of photogenerated charges [27]. Similarly, Pd_2Cu/TiO_2 catalyst gave an ethanol production rate of 4.1 mmol g^{-1} h^{-1} at 150 °C under visible light irradiation [85]. The plasmonic properties of Pd_2Cu, the CO_2 adsorption capacity of Cu, and the oxidation and C-C bond formation competence of Pd accounted for its performance [85].

4. Other Catalysts

In addition to semiconductor- and plasmonic metal-based catalysts, Co-based catalysts and Pd-based catalysts have also been studied in photocatalytic CO_2 reduction to ethanol. In this section, we will review the progress of these two types of photocatalysts for CO_2 reduction reactions.

4.1. Co-Based Catalysts

In thermal-driven reaction systems, Co is one of the active metals for C-C coupling reactions [86,87]. The competence of Co active sites for the formation of C-C bond endows Co-based catalysts applicability in the photocatalytic CO_2 reduction to ethanol [88,89]. For instance, Na-modified Co@C nanocomposite catalyst gave almost 100% selectivity to hydrocarbons and ~6% selectivity towards ethanol at 235 °C and under the irradiation of a solar simulator. Mechanism study revealed that, upon light irradiation, photoexcited charges were generated on Na-Co@C, which facilitated the formation of electron-rich carbon species. These species were further involved in CO_2 activation to ${CO_2}^{\delta-}$ and promoted the dissociation of CO_2 to CO. The CO was stabilized by the carbon layers on Na-Co@C, and produced ethanol via a CO insertion pathway [88].

4.2. Pd-Based Catalysts

The PdIn@N_3-COF (N_3-COF is a photosensitizing covalent organic framework) [90] and Pd/Mn-TiO_2 [91] catalysts have also been successfully utilized in photocatalytic CO_2 reduction to ethanol. Here, PdIn@N_3-COF is taken as an example for elaboration. Lu et al. confined bimetallic PdIn nanoclusters in N_3-COF to construct a PdIn@N_3-COF composite, and investigated its performance in photocatalytic CO_2 reduction to ethanol [90]. It revealed that PdIn@N_3-COF gave a total yield toward alcohols of 33.3 μmol g^{-1} h^{-1} and a selectivity to ethanol of 26%. On the one hand, the interaction between PdIn and N_3-COF facilitated the charge transfer; on the other hand, the bimetallic synergistic effect of PdIn-stabilized C_1 intimidates C-C coupling while retaining some of the C-O bonds. Both of these two factors contributed to the high conversion of CO_2 to ethanol [90].

5. Summary and Outlook

Up to now, a number of catalysts have been designed for photocatalytic CO_2 reduction to ethanol, including semiconductors, plasmonic-metal based catalysts, and several other catalysts (a brief summary of some typical catalysts is shown in Table 1). Clearly, in spite of the rapid progress, several challenges remain.

Table 1. Brief summary of some typical catalysts for photocatalytic CO_2 reduction to ethanol.

Catalyst Category	Catalyst	Reaction Condition	Performance	Ref.
Pristine semiconductors	TiO_2	Reactor—home-made glass reactor, 50 mm in diameter and 100 mm in height; Reactant—10 mL deionized water and water saturated CO_2; Light source—100 W Xe lamp, 35 mW cm^{-2}.	Ethanol formation rate of ~9.0 nmol cm^{-2} h^{-1}.	[23]
Pristine semiconductors	Bi_2MoO_6	Reactor—closed vessel; reactant—50 mL deionized water and saturated CO_2; Light source—300 W Xe arc lamp (PLS-SXE300) with an ultraviolet cutoff filter ($\lambda \geq 420$ nm).	Ethanol yield of 4.7 μmol g^{-1} h^{-1}.	[34]
Semiconductors with vacancy sites	Reduced $HCa_2Ta_3O_{10}$	Reactor—an in situ closed circulation system; Reactant—CO_2 saturated with H_2O vapor; Light source—150 W Xe arc lamp, 100 mW cm^{-2}.	Ethanol yield of 113.0 μmol g^{-1} h^{-1}.	[43]
Heterojunctions	TiO_2/Ti_3C_2	Reactor—two electrode system; Reactant—0.1 M $KHCO_3$ aqueous solution (pH = 6.8, 50 mL) saturated by CO_2; Light source—300 W xenon lamp (PLS-SXE300/300UV) with 200 mW cm^{-2} light intensity; External bias potential—-0.6 V.	Ethanol formation rate of ~10.0 μmol cm^{-2} h^{-1}.	[50]
Heterojunctions	$TiO_2/rGO/CeO_2$	Reactor—sealed photocatalytic reactor; Reactant—150 mL distilled water with saturated CO_2; Light source—UV light (a 15 W UV-C mercury lamp, peak light intensity 254 nm); Catalyst—0.15 g.	Ethanol yield of 271.0 μmol g^{-1} h^{-1}.	[54]
Hybrid catalysts constructed between a semiconductor and a non-semiconductor material	WS_2 QD/Bi_2S_3	Reactor—closed 200 mL quartz glass reactor; Reactant—50 mL of ultrapure water with saturated CO_2; Light source—300 W Xe arc lamp (PLS-SXE300).	Ethanol yield of 7.0 μmol g^{-1} h^{-1}.	[57]
Hybrid catalysts constructed between a semiconductor and a non-semiconductor material	g-C_3N_4/CuO@MIL-125(Ti)	Reactor—visual micro autoclave lined with 100 mL polytetrafluoroethylene; Reactant—1.0 mL water and 0.3% CO_2; Pressure—1.0 MPa; Light source—300 W Xe lamp, 326.1W m^{-2}.	Ethanol yield of 501.9 μmol g^{-1} h^{-1}.	[63]
Cu-based catalysts	$SrTiO_3$/Cu@Ni/TiN	Reactor—Labsolar 6 A system (Beijing Perfectlight Technology Co., Ltd.); Reactant—10 mL ultrapure water and saturated CO_2; Light source—300 W Xe lamp, 600 mW cm^{-2}.	Ethanol yield of 21.3 μmol g^{-1} h^{-1} and an ethanol selectivity of 79%.	[75]
Ag-based catalysts	Ag@AgBr/CNT	Reactor—stainless steel vessel; Reactant—100 mL 0.2 M $KHCO_3$ solution, pure CO_2 (99.99%) with a pressure of 7.5 MPa; Light source—A 150 W Xe lamp (Shanghai Aojia Lighting Appliance Co. Ltd.) with UV cutoff filter ($\lambda > 420$ nm).	Ethanol yield of 5.0 μmol g^{-1} h^{-1}.	[81]

Table 1. *Cont.*

Catalyst Category	Catalyst	Reaction Condition	Performance	Ref.
Au-based catalysts	Au/ZIF-67	Reactor—horizontal-glass-type photoreactor; Reactant—10 mL of aqueous solution with 10 wt % triethanolamine, 67 mg $NaHCO_3$, purged with CO_2; Light source—Abet 103 with light intensity fixed at 150 mW cm^{-2}.	Ethanol yield of 0.5 mmol g^{-1} h^{-1}.	[83]
Plasmonic alloy-based catalysts	AuCu/g-C_3N_4	Reactor—high-temperature and-high pressure CEL-HPR reactor with a volume of 250 mL (Beijing Zhongjiao Jinyuan Technology Co., Ltd.); Reactant—100 mL ultrapure water, high-purity CO_2 (99.999%), 0.8 MPa; Light source—300 W Xe lamp ($\lambda > 420$ nm), Temperature—80–160 °C.	An ethanol yield and selectivity of 0.9 mmol g^{-1} h^{-1} and 93.1%, respectively.	[27]
Co-based catalysts	Na-Co@C	Reactor—quartz cell reactor; Reactant—CO_2, N_2, and H_2 of 20, 20, and 100 cm^3 at standard conditions, with a final pressure of ~2.8 bar; Light source—Xe lamp (1000 W) coupled with an AM1.5 filter; Temperature—235 °C.	~6% selectivity towards ethanol.	[88]
Pd-based catalysts	PdIn@N_3-COF	Reactor—double-walled 80 mL quartz photoreactor; Reactant—10 mL ultrapure water with saturated CO_2; Light source—300 W Xe lamp (CEL-HXF300, CEAULICHT) with a 400 nm filter.	A total yield toward alcohols of 33.3 μmol g^{-1} h^{-1} and a selectivity to ethanol of 26%.	[90]

(1) CO_2 conversion rates over most of the catalysts are still low.

At present, semiconductors in photocatalytic CO_2 conversion to ethanol mainly face the following challenges: ① most semiconductors have a relatively low response to light due to the limitation of their own electronic structures, and ② photogenerated electron–hole pairs in semiconductors combine relatively quickly. These challenges result in ineffective performance of semiconductors in CO_2 photoreduction to ethanol. In terms of plasmonic metal-based catalysts, the absorption of light by plasmonic metal nanoparticles is mainly concentrated in the range of the ultraviolet light and visible light region, which makes the light utilization efficiency very low and leads to poor performance.

Due to these reasons, over most of the studied catalysts, CO_2 conversion rates are in the magnitude of μmol g^{-1} h^{-1}. Even though some catalysts could record CO_2 conversion rates up to mmol g^{-1} h^{-1}, this is still far away from what is required for industrialization applications. Therefore, there is still a long way to accelerate CO_2 conversion rates. Developing catalysts with high efficiencies for CO_2 activation or establishing photothermal catalytic systems to enhance CO_2 conversion might be future research pathways. For instance, it has been reported that surface site engineering of semiconductors is beneficial to increase the absorption range of light and to enhance the separation of photogenerated electrons and holes, thereby promoting the surface redox reaction and improving the photocatalytic CO_2 reduction to methanol, methane, CO, and others [92,93]. Adopting the surface site engineering strategy to develop suitable catalysts for CO_2 photoreduction to ethanol might be promising approach to enhance the CO_2 conversion rates.

(2) The selectivity towards ethanol needs improvement.

Photocatalytic CO_2 reduction to ethanol requires multiple electrons of strong energies [94,95]. The requirements are more critical than CO_2 photoreduction to CO, methane, methanol, and so on, which makes it difficult to realize 100% selectivity towards ethanol. Therefore, developing catalysts with tailored properties which could selectively produce

ethanol is one of the challenges in this study. It has been reported that single atom catalysts are of specific geometric and electronic structures, which limits the absorption geometry of reactants on the catalytic active sites and is beneficial to providing product selectively. Therefore, delicately designing single atom catalysts or catalysts with specified sizes might be avenue to improve the selectivity towards ethanol.

(3) Some plasmonic metal-based catalysts are expensive.

Currently, the plasmonic metal-based catalysts used in photocatalytic CO_2 conversion to ethanol are mainly focused on precious metals, such as gold and silver. These noble metals are expensive and deactivate easily due to sintering. Therefore, non-noble metal-based plasmonic catalysts should be developed, such as Cu, Al, and some transition oxides with plasmonic properties. With the help of the above two prospects to enhance the CO_2 conversion rate and improve the selectivity towards ethanol, if these non-noble metal-based plasmonic catalysts are of high catalytic performance in CO_2 photoreduction to ethanol, it will be of stronger practical significance.

(4) The reaction mechanism is still unclear.

Most of the current studies focus on catalyst design and the improvement of ethanol production, whereas the underlying reaction mechanisms are not extensively investigated. Making clear the reaction mechanism could provide guidance for the rational design of efficient catalysts in the future. Combining the advanced in situ techniques (such as high-angle annular dark field scanning transmission electron microscopy, extended X-ray absorption fine structure, X-ray absorption near-edge structure, diffuse reflectance infrared Fourier transform spectroscopy, atmospheric pressure X-ray photoelectron spectroscopy), and theoretical calculations (density functional theory), might be avenues to unravel the underlying mechanisms.

Author Contributions: Writing—original draft preparation, D.L.; writing—review and editing, C.H.; guidance, supervision and project administration, H.L.; visualization, Conceptualization, R.Z. and Y.L.; software, J.G. (Jiawen Guo); formal analysis, J.G. (Jiapeng Guo); resources, C.C.V.; All authors have read and agreed to the published version of the manuscript.

Funding: National Natural Science Foundation of China (21902116) and the Education Department of Liaoning Province (JQL202015401).

Data Availability Statement: We can provide the data upon requirements.

Conflicts of Interest: The authors declare no conflict of interest.

References

1. Das, S.; Pérez-Ramírez, J.; Gong, J.; Dewangan, N.; Hidajat, K.; Gates, B.C.; Kawi, S. Core-shell structured catalysts for thermocatalytic, photocatalytic, and electrocatalytic conversion of CO_2. *Chem. Soc. Rev.* **2020**, *49*, 2937–3004. [CrossRef] [PubMed]
2. Singh, G.; Lee, J.; Karakoti, A.; Bahadur, R.; Yi, J.; Zhao, D.; AlBahily, K.; Vinu, A. Emerging trends in porous materials for CO_2 capture and conversion. *Chem. Soc. Rev.* **2020**, *49*, 4360–4404. [CrossRef]
3. Masel, R.I.; Liu, Z.; Yang, H.; Kaczur, J.; Carrillo, D.; Ren, S.; Salvatore, D.; Berlinguette, C. An industrial perspective on catalysts for low-temperature CO_2 electrolysis. *Nat. Nanotechnol.* **2021**, *16*, 118–128. [CrossRef] [PubMed]
4. Wang, D.; Bi, Q.; Yin, G.; Wang, P.; Huang, F.; Xie, X.; Jiang, M. Photochemical preparation of anatase titania supported gold catalyst for ethanol synthesis from CO_2 hydrogenation. *Catal. Lett.* **2018**, *148*, 11–22. [CrossRef]
5. Wang, J.; Han, B.; Nie, R.; Xu, Y.; Yu, X.; Dong, Y.; Wang, J.; Jing, H. Photoelectrocatalytic reduction of CO_2 to chemicals via ZnO@ nickel foam: Controlling C-C coupling by ligand or morphology. *Top. Catal.* **2018**, *61*, 1563–1573. [CrossRef]
6. Wang, Z.J.; Song, H.; Liu, H.; Ye, J. Coupling of solar energy and thermal energy for carbon dioxide reduction: Status and prospects. *Angew. Chem. Int. Ed.* **2020**, *59*, 8016–8035. [CrossRef]
7. Zhang, W.; Mohamed, A.R.; Ong, W.J. Z-Scheme photocatalytic systems for carbon dioxide reduction: Where are we now? *Angew. Chem. Int. Ed.* **2020**, *59*, 22894–22915. [CrossRef] [PubMed]
8. Dong, W.-H.; Wu, D.-D.; Luo, J.-M.; Xing, Q.-J.; Liu, H.; Zou, J.-P.; Luo, X.-B.; Min, X.-B.; Liu, H.-L.; Luo, S.-L. Coupling of photodegradation of RhB with photoreduction of CO_2 over rGO/$SrTi_{0.95}Fe_{0.005}O_3$−delta catalyst: A strategy for one-pot conversion of organic pollutants to methanol and ethanol. *J. Catal.* **2017**, *349*, 218–225. [CrossRef]
9. Jeyalakshmi, V.; Tamilmani, S.; Mahalakshmy, R.; Bhyrappa, P.; Krishnamurthy, K.R.; Viswanathan, B. Sensitization of La modified $NaTaO_3$ with cobalt tetra phenyl porphyrin for photo catalytic reduction of CO_2 by water with UV–visible light. *J. Mol. Catal. A-Chem.* **2016**, *420*, 200–207. [CrossRef]

10. Liu, H.; Meng, X.; Dao, T.D.; Zhang, H.; Li, P.; Chang, K.; Wang, T.; Li, M.; Nagao, T.; Ye, J. Conversion of carbon dioxide by methane reforming under visible-light irradiation: Surface-plasmon-mediated nonpolar molecule activation. *Angew. Chem. Int. Ed.* **2015**, *127*, 11707–11711. [CrossRef]
11. Liu, H.; Dao, T.D.; Liu, L.; Meng, X.; Nagao, T.; Ye, J. Light assisted CO_2 reduction with methane over group VIII metals: Universality of metal localized surface plasmon resonance in reactant activation. *Appl. Catal. B Environ.* **2017**, *209*, 183–189. [CrossRef]
12. Liu, H.; Li, M.; Dao, T.D.; Liu, Y.; Zhou, W.; Liu, L.; Meng, X.; Nagao, T.; Ye, J. Design of PdAu alloy plasmonic nanoparticles for improved catalytic performance in CO_2 reduction with visible light irradiation. *Nano Energy* **2016**, *26*, 398–404. [CrossRef]
13. Zhao, Y.; Wei, Y.; Wu, X.; Zheng, H.; Zhao, Z.; Liu, J.; Li, J. Graphene-wrapped Pt/TiO_2 photocatalysts. with enhanced photogenerated charges separation and reactant adsorption for high selective photoreduction of CO_2 to CH_4. *Appl. Catal. B Environ.* **2018**, *226*, 360–372. [CrossRef]
14. Li, X.; Sun, Y.; Xu, J.; Shao, Y.; Wu, J.; Xu, X.; Pan, Y.; Ju, H.; Zhu, J.; Xie, Y. Selective visible-light-driven photocatalytic CO_2 reduction to CH_4 mediated by atomically thin CuIn5S8 layers. *Nat. Energy* **2019**, *4*, 690–699. [CrossRef]
15. Wu, Y.A.; McNulty, I.; Liu, C.; Lau, K.C.; Liu, Q.; Paulikas, A.P.; Sun, C.-J.; Cai, Z.; Guest, J.R.; Ren, Y. Facet-dependent active sites of a single Cu_2O particle photocatalyst for CO_2 reduction to methanol. *Nat. Energy* **2019**, *4*, 957–968. [CrossRef]
16. Chen, G.; Waterhouse, G.I.; Shi, R.; Zhao, J.; Li, Z.; Wu, L.Z.; Tung, C.H.; Zhang, T. From solar energy to fuels: Recent advances in light-driven C1 chemistry. *Angew. Chem. Int. Ed.* **2019**, *58*, 17528–17551. [CrossRef]
17. Singh, M.R.; Bell, A.T. Design of an artificial photosynthetic system for production of alcohols in high concentration from CO_2. *Energy Environ. Sci.* **2016**, *9*, 193–199. [CrossRef]
18. Sans, J.; Sanz, V.; Turon, P.; Alemán, C. Enhanced CO_2 conversion into ethanol by permanently polarized hydroxyapatite through C-C Coupling. *ChemCatChem* **2021**, *13*, 5025–5033. [CrossRef]
19. Usubharatana, P.; McMartin, D.; Veawab, A.; Tontiwachwuthikul, P. Photocatalytic process for CO_2 emission reduction from industrial flue gas streams. *Ind. Eng. Chem. Res.* **2006**, *45*, 2558–2568. [CrossRef]
20. Jeyalakshmi, V.; Mahalakshmy, R.; Krishnamurthy, K.R.; Viswanathan, B. Photocatalytic reduction of carbon dioxide in alkaline medium on La modified sodium tantalate with different CO-Catalysts. under UV–Visible radiation. *Catal. Today* **2016**, *266*, 160–167. [CrossRef]
21. Li, D.; Kassymova, M.; Cai, X.; Zang, S.-Q.; Jiang, H.-L. Photocatalytic CO_2 reduction over metal-organic framework-based materials. *Coord. Chem. Rev.* **2020**, *412*, 213262. [CrossRef]
22. Kumaravel, V.; Bartlett, J.; Pillai, S.C. Photoelectrochemical conversion of carbon dioxide (CO_2) into fuels and value-added products. *ACS Energy Lett.* **2020**, *5*, 486–519. [CrossRef]
23. Ping, G.; Wang, C.; Chen, D.; Liu, S.; Huang, X.; Qin, L.; Huang, Y.; Shu, K. Fabrication of self-organized TiO_2 nanotube arrays for photocatalytic reduction of CO_2. *J. Solid State Electr.* **2013**, *17*, 2503–2510. [CrossRef]
24. Ribeiro, C.S.; Lansarin, M.A. Enhanced photocatalytic activity of Bi_2WO_6 with PVP addition for CO_2 reduction into ethanol under visible light. *Environ. Sci. Pollut. R* **2021**, *28*, 23667–23674. [CrossRef]
25. Li, F.; Zhang, D.; Xiang, Q. Nanosheet-assembled hierarchical flower-like g-C_3N_4 for enhanced photocatalytic CO_2 reduction activity. *Chem. Commun.* **2020**, *56*, 2443–2446. [CrossRef] [PubMed]
26. Cheng, M.; Yang, S.; Chen, R.; Zhu, X.; Liao, Q.; Huang, Y. Copper-decorated TiO_2 nanorod thin films in optofluidic planar reactors for efficient photocatalytic reduction of CO_2. *Int. J. Hydrogen Energy* **2017**, *42*, 9722–9732. [CrossRef]
27. Li, P.; Liu, L.; An, W.; Wang, H.; Guo, H.; Liang, Y.; Cui, W. Ultrathin porous g-C_3N_4 nanosheets modified with AuCu alloy nanoparticles and C-C coupling photothermal catalytic reduction of CO_2 to ethanol. *Appl. Catal. B Environ.* **2020**, *266*, 118618. [CrossRef]
28. Habisreutinger, S.N.; Schmidt Mende, L.; Stolarczyk, J.K. Photocatalytic reduction of CO_2 on TiO_2 and other semiconductors. *Angew. Chem. Int. Ed.* **2013**, *52*, 7372–7408. [CrossRef]
29. Li, X.; Wen, J.; Low, J.; Fang, Y.; Yu, J. Design and fabrication of semiconductor photocatalyst for photocatalytic reduction of CO_2 to solar fuel. *Sci. China Mater.* **2014**, *57*, 70–100. [CrossRef]
30. Amrillah, T.; Supandi, A.R.; Puspasari, V.; Hermawan, A.; Seh, Z.W. MXene-based photocatalysts and electrocatalysts for CO_2 conversion to chemicals. *Trans. Tianjin Univ.* **2022**, *4*, 307–322. [CrossRef]
31. Cheng, S.; Sun, Z.; Lim, K.H.; Gani, T.Z.H.; Zhang, T.; Wang, Y.; Yin, H.; Liu, K.; Guo, H.; Du, T. Emerging strategies for CO_2 photoreduction to CH_4: From experimental to data-driven design. *Adv. Energy Mater.* **2022**, *12*, 2200389. [CrossRef]
32. Chang, X.; Wang, T.; Gong, J. CO_2 photo-reduction: Insights into CO_2 activation and reaction on surfaces of photocatalysts. *Energy Environ. Sci.* **2016**, *9*, 2177–2196. [CrossRef]
33. Song, Y.; Chen, W.; Wei, W.; Sun, Y. Advances in clean fuel ethanol production from electro-, photo- and photoelectro-catalytic CO_2 Reduction. *Catalysts* **2020**, *10*, 1287. [CrossRef]
34. Dai, W.; Yu, J.; Xu, H.; Hu, X.; Luo, X.; Yang, L.; Tu, X. Synthesis of hierarchical flower-like Bi_2MoO_6 microspheres as efficient photocatalyst for photoreduction of CO_2 into solar fuels under visible light. *Crystengcomm* **2016**, *18*, 3472–3480. [CrossRef]
35. Ribeiro, C.S.; Lansarin, M.A. Facile solvo-hydrothermal synthesis of Bi_2MoO_6 for the photocatalytic reduction of CO_2 into ethanol in water under visible light. *React. Kinet. Mech. Cat.* **2019**, *127*, 1059–1071. [CrossRef]
36. Liu, Y.; Huang, B.; Dai, Y.; Zhang, X.; Qin, X.; Jiang, M.; Whangbo, M.-H. Selective ethanol formation from photocatalytic reduction of carbon dioxide in water with $BiVO_4$ photocatalyst. *Catal. Commun.* **2009**, *11*, 210–213. [CrossRef]

37. Sanchez-Rodriguez, D.; Berenice Jasso-Salcedo, A.; Hedin, N.; Church, T.L.; Aizpuru, A.; Alonso Escobar-Barrios, V. Semiconducting nanocrystalline Bismuth Oxychloride (BiOCl) for Photocatalytic Reduction of CO_2. *Catalysts* **2020**, *10*, 998. [CrossRef]
38. Han, Q.; Zhou, Y.; Tang, L.; Li, P.; Tu, W.; Li, L.; Lia, H.; Zou, Z. Synthesis of single-crystalline, porous TaON microspheres toward visible-light photocatalytic conversion of CO_2 into liquid hydrocarbon fuels. *RSC Adv.* **2016**, *6*, 90792–90796. [CrossRef]
39. Ashiq, M.N.; Wang, Y.; Ehsan, M.F.; He, T. Photoreduction of carbon dioxide using strontium zirconate nanoparticles. *Sci. China Mater.* **2015**, *58*, 634–639.
40. Meng, A.; Zhang, L.; Cheng, B.; Yu, J. Dual cocatalysts in TiO_2 photocatalysis. *Adv. Mater.* **2019**, *31*, 1807660. [CrossRef]
41. Shayegan, Z.; Lee, C.-S.; Haghighat, F. TiO_2 photocatalyst for removal of volatile organic compounds in gas phase-A review. *Chem. Eng. J.* **2018**, *334*, 2408–2439. [CrossRef]
42. Dai, W.; Long, J.; Yang, L.; Zhang, S.; Xu, Y.; Luo, X.; Zou, J.; Luo, S. Oxygen migration triggering molybdenum exposure in oxygen vacancy-rich ultra-thin Bi_2MoO_6 nanoflakes: Dual binding sites governing selective CO_2 reduction into liquid hydrocarbons. *J. Energy Chem.* **2021**, *61*, 281–289. [CrossRef]
43. Nhu-Nang, V.; Chinh-Chien, N.; Kaliaguine, S.; Trong-On, D. Reduced Cu/Pt-$HCa_2Ta_3O_{10}$ perovskite nanosheets for sunlight-driven conversion of CO_2 into valuable fuels. *Adv. Sustain. Syst.* **2017**, *1*, 1700048.
44. Wang, Q.; Wang, X.; Yu, Z.; Jiang, X.; Chen, J.; Tao, L.; Wang, M.; Shen, Y. Artificial photosynthesis of ethanol using type-II g-C_3N_4/ZnTe heterojunction in photoelectrochemical CO_2 reduction system. *Nano Energy* **2019**, *60*, 827–835. [CrossRef]
45. Li, P.; Liu, L.; An, W.; Wang, H.; Cui, W. Efficient photothermal catalytic CO_2 reduction to CH_3CH_2OH over Cu_2O/g-C_3N_4 assisted by ionic liquids. *Appl. Surf. Sci.* **2021**, *565*, 150448. [CrossRef]
46. Huang, Y.; Yan, C.-F.; Guo, C.-Q.; Huang, S.-L. Enhanced photoreduction activity of carbon dioxide over Co_3O_4/CeO_2 catalysts under visible light irradiation. *Int. J. Photoenergy* **2015**, *2015*, 230808. [CrossRef]
47. Dai, W.; Yu, J.; Deng, Y.; Hu, X.; Wang, T.; Luo, X. Facile synthesis of MoS_2/Bi_2WO_6 nanocomposites for enhanced CO_2 photoreduction activity under visible light irradiation. *Appl. Surf. Sci.* **2017**, *403*, 230–239. [CrossRef]
48. Meng, A.; Wu, S.; Cheng, B.; Yu, J.; Xu, J. Hierarchical TiO_2/$Ni(OH)_2$ composite fibers with enhanced photocatalytic CO_2 reduction performance. *J. Mater. Chem. A* **2018**, *6*, 4729–4736. [CrossRef]
49. Zhao, D.; Xuan, Y.; Zhang, K.; Liu, X. Highly selective production of ethanol over hierarchical Bi@Bi_2MoO_6 composite via bicarbonate-assisted photocatalytic CO_2 reduction. *Chemsuschem* **2021**, *14*, 3293–3302. [CrossRef]
50. Xu, Y.; Wang, S.; Yang, J.; Han, B.; Nie, R.; Wang, J.; Wang, J.; Jing, H. In-situ grown nanocrystal TiO_2 on 2D Ti_3C_2 nanosheets for artificial photosynthesis of chemical fuels. *Nano Energy* **2018**, *51*, 442–450. [CrossRef]
51. Li, H.; Li, C.; Han, L.; Li, C.; Zhang, S. Photocatalytic reduction of CO_2 with H_2O on CuO/TiO_2 catalysts. *Energy Sources Part A* **2016**, *38*, 420–426. [CrossRef]
52. Abou Asi, M.; He, C.; Su, M.; Xia, D.; Lin, L.; Deng, H.; Xiong, Y.; Qiu, R.; Li, X.-z. Photocatalytic reduction of CO_2 to hydrocarbons using AgBr/TiO_2 nanocomposites under visible light. *Catal. Today* **2011**, *175*, 256–263. [CrossRef]
53. Korovin, E.; Selishchev, D.; Kozlov, D. Photocatalytic CO_2 reduction on the TiO_2 P25 under the high power UV-LED irradiation. *Top. Catal.* **2016**, *59*, 1292–1296. [CrossRef]
54. Seeharaj, P.; Kongmun, P.; Paiplod, P.; Prakobmit, S.; Sriwong, C.; Kim-Lohsoontorn, P.; Vittayakorn, N. Ultrasonically-assisted surface modified TiO_2/rGO/CeO_2 heterojunction photocatalysts for conversion of CO_2 to methanol and ethanol. *Ultrason. Sonochem.* **2019**, *58*, 104657. [CrossRef] [PubMed]
55. Wei, Y.; Cheng, Z.; Lin, J. An overview on enhancing the stability of lead halide perovskite quantum dots and their applications in phosphor-converted LEDs. *Chem. Soc. Rev.* **2019**, *48*, 310–350. [CrossRef] [PubMed]
56. Yan, Y.; Gong, J.; Chen, J.; Zeng, Z.; Huang, W.; Pu, K.; Liu, J.; Chen, P. Recent advances on graphene quantum dots: From chemistry and physics to applications. *Adv. Mater.* **2019**, *31*, 1808283. [CrossRef]
57. Dai, W.; Yu, J.; Luo, S.; Hu, X.; Yang, L.; Zhang, S.; Li, B.; Luo, X.; Zou, J. WS_2 quantum dots seeding in Bi_2S_3 nanotubes: A novel Vis-NIR light sensitive photocatalyst with low-resistance junction interface for CO_2 reduction. *Chem. Eng. J.* **2020**, *389*, 123430. [CrossRef]
58. Dai, W.; Xiong, W.; Yu, J.; Zhang, S.; Li, B.; Yang, L.; Wang, T.; Luo, X.; Zou, J.; Luo, S. Bi_2MoO_6 quantum dots in situ grown on reduced graphene oxide layers: A novel electron-rich interface for efficient CO_2 reduction. *ACS Appl. Mater. Interfaces* **2020**, *12*, 25861–25874. [CrossRef]
59. Cheng, M.; Yang, S.; Chen, R.; Zhu, X.; Liao, Q.; Huang, Y. Visible light responsive CdS sensitized TiO_2 nanorod array films for efficient photocatalytic reduction of gas phase CO_2. *Mol. Catal.* **2018**, *448*, 185–194. [CrossRef]
60. Xiao, J.-D.; Jiang, H.-L. Metal-organic frameworks for photocatalysis and photothermal catalysis. *Acc. Chem. Res.* **2018**, *52*, 356–366. [CrossRef]
61. Xiao, X.; Zou, L.; Pang, H.; Xu, Q. Synthesis of micro/nanoscaled metal-organic frameworks and their direct electrochemical applications. *Chem. Soc. Rev.* **2020**, *49*, 301–331. [CrossRef] [PubMed]
62. Meng, Y.; Zhang, L.; Jiu, H.; Zhang, Q.; Zhang, H.; Ren, W.; Sun, Y.; Li, D. Construction of g-C_3N_4/ZIF-67 photocatalyst with enhanced photocatalytic CO_2 reduction activity. *Mat. Sci. Semicon. Proc.* **2019**, *95*, 35–41. [CrossRef]
63. Li, N.; Liu, X.; Zhou, J.; Chen, W.; Liu, M. Encapsulating CuO quantum dots in MIL-125(Ti) coupled with g-C_3N_4 for efficient photocatalytic CO_2 reduction. *Chem. Eng. J.* **2020**, *399*, 125782. [CrossRef]

64. Cardoso, J.; Stulp, S.; De Brito, J.; Flor, J.; Frem, R.; Zanoni, M. MOFs based on ZIF-8 deposited on TiO_2 nanotubes increase the surface adsorption of CO_2 and its photoelectrocatalytic reduction to alcohols in aqueous media. *Appl. Catal. B Environ.* **2018**, *225*, 563–573. [CrossRef]
65. Dai, W.; Xu, H.; Yu, J.; Hu, X.; Luo, X.; Tu, X.; Yang, L. Photocatalytic reduction of CO_2 into methanol and ethanol over conducting polymers modified Bi_2WO_6 microspheres under visible light. *Appl. Surf. Sci.* **2015**, *356*, 173–180. [CrossRef]
66. Pastrana-Martínez, L.; Silva, A.; Fonseca, N.; Vaz, J.; Figueiredo, J.; Faria, J. Photocatalytic reduction of CO_2 with water into methanol and ethanol using graphene derivative-TiO_2 composites: Effect of pH and copper (I) oxide. *Top. Catal.* **2016**, *59*, 1279–1291. [CrossRef]
67. Wang, L.; Wei, Y.; Fang, R.; Wang, J.; Yu, X.; Chen, J.; Jing, H. Photoelectrocatalytic CO_2 reduction to ethanol via graphite-supported and functionalized TiO_2 nanowires photocathode. *J. Photoch. Photobio. A* **2020**, *391*, 112368. [CrossRef]
68. Wang, Y.; Jia, H.; Gong, H.; Zhou, L.; Qiu, Z.; Fang, X.; Du, T. Fabrication of trimodal porous silica/g-C_3N_4 nanotubes for efficient visible light photocatalytic reduction of CO_2 to ethanol. *Chem. Eng. J.* **2021**, *426*, 130877. [CrossRef]
69. Maimaitizi, H.; Abulizi, A.; Kadeer, K.; Talifu, D.; Tursun, Y. In situ synthesis of Pt and N co-doped hollow hierarchical BiOCl microsphere as an efficient photocatalyst for organic pollutant degradation and photocatalytic CO_2 reduction. *Appl. Surf. Sci.* **2020**, *502*, 144083. [CrossRef]
70. Li, N.; Li, Y.; Jiang, R.; Zhou, J.; Liu, M. Photocatalytic coupling of methane and CO_2 into C2-hydrocarbons over Zn doped g-C_3N_4 catalysts. *Appl. Surf. Sci.* **2019**, *498*, 143861. [CrossRef]
71. Aslam, U.; Rao, V.G.; Chavez, S.; Linic, S. Catalytic conversion of solar to chemical energy on plasmonic metal nanostructures. *Nat. Catal.* **2018**, *1*, 656–665. [CrossRef]
72. Agrawal, A.; Cho, S.H.; Zandi, O.; Ghosh, S.; Johns, R.W.; Milliron, D.J. Localized surface plasmon resonance in semiconductor nanocrystals. *Chem. Rev.* **2018**, *118*, 3121–3207. [CrossRef]
73. Vu, N.N.; Kaliaguine, S.; Do, T.O. Plasmonic photo catalysts for sunlight-driven reduction of CO_2: Details, developments, and perspectives. *Chemsuschem* **2020**, *13*, 3967–3991. [CrossRef]
74. Li, S.; Miao, P.; Zhang, Y.; Wu, J.; Zhang, B.; Du, Y.; Han, X.; Sun, J.; Xu, P. Recent advances in plasmonic nanostructures for enhanced photocatalysis and electrocatalysis. *Adv. Mater.* **2021**, *33*, 2000086. [CrossRef]
75. Yu, H.; Sun, C.; Xuan, Y.; Zhang, K.; Chang, K. Full solar spectrum driven plasmonic-assisted efficient photocatalytic CO_2 reduction to ethanol. *Chem. Eng. J.* **2022**, *430*, 132940. [CrossRef]
76. Lertthanaphol, N.; Pienutsa, N.; Chusri, K.; Sornsuchat, T.; Chanthara, P.; Seeharaj, P.; Kim-Lohsoontorn, P.; Srinives, S. One-step hydrothermal synthesis of precious metal-doped Titanium dioxide-graphene oxide composites for photocatalytic conversion of CO_2 to ethanol. *ACS Omega* **2021**, *6*, 35769–35779. [CrossRef] [PubMed]
77. Zeng, L.Z.; Wang, Z.Y.; Wang, Y.K.; Wang, J.; Guo, Y.; Hu, H.H.; He, X.F.; Wang, C.; Lin, W.B. Photoactivation of Cu centers in metal-organic frameworks for selective CO_2 conversion to ethanol. *J.Am.Chem.Soc.* **2020**, *142*, 75–79. [CrossRef]
78. Wang, G.; He, C.T.; Huang, R.; Mao, J.J.; Wang, D.S.; Li, Y.D. Photoinduction of Cu single atoms decorated on UiO-66-NH_2 for enhanced photocatalytic reduction of CO_2 to liquid fuels. *J.Am.Chem.Soc.* **2020**, *142*, 19339–19345. [CrossRef]
79. Almomani, F.; Bhosale, R.; Khraisheh, M.; Kumar, A.; Tawalbeh, M. Photocatalytic conversion of CO_2 and H_2O to useful fuels by nanostructured composite catalysis. *Appl. Surf. Sci.* **2019**, *483*, 363–372. [CrossRef]
80. Lu, Y.; Cao, H.; Xu, S.; Feng, W.; Hou, G.; Tang, Y.; Zhang, H.; Zheng, G. CO_2 photoelectroreduction with enhanced ethanol selectivity by high valence rhenium-doped copper oxide composite catalysts. *J. Colloid Interface Sci.* **2021**, *599*, 497–506. [CrossRef] [PubMed]
81. Abou Asi, M.; Zhu, L.; He, C.; Sharma, V.K.; Shu, D.; Li, S.; Yang, J.; Xiong, Y. Visible-light-harvesting reduction of CO_2 to chemical fuels with plasmonic Ag@AgBr/CNT nanocomposites. *Catal. Today* **2013**, *216*, 268–275. [CrossRef]
82. An, C.; Wang, J.; Qin, C.; Jiang, W.; Wang, S.; Li, Y.; Zhang, Q. Synthesis of Ag@AgBr/AgCl heterostructured nanocashews with enhanced photocatalytic performance via anion exchange. *J. Mater. Chem.* **2012**, *22*, 13153–13158. [CrossRef]
83. Becerra, J.; Duc-Trung, N.; Gopalakrishnan, V.-N.; Trong-On, D. Plasmonic Au nanoparticles incorporated in the zeolitic Imidazolate Framework (ZIF-67) for the efficient sunlight-driven photoreduction of CO_2. *ACS Appl. Energy Mater.* **2020**, *3*, 7659–7665. [CrossRef]
84. Compagnoni, M.; Villa, A.; Bandori, E.; Morgan, D.J.; Prati, L.; Dimitratos, N.; Rossetti, I.; Ramis, G. Surface probing by spectroscopy on titania-supported gold nanoparticles for a photoreductive application. *Catalysts* **2018**, *8*, 623. [CrossRef]
85. Elavarasan, M.; Yang, W.; Velmurugan, S.; Chen, J.-N.; Yang, T.C.K.; Yokoi, T. Highly efficient photothermal reduction of CO_2 on Pd_2Cu dispersed TiO_2 photocatalyst and operando DRIFT spectroscopic analysis of reactive intermediates. *Nanomaterials* **2022**, *12*, 332. [CrossRef]
86. Guérinot, A.; Cossy, J. Cobalt-catalyzed cross-couplings between alkyl halides and grignard reagents. *Acc. Chem. Res.* **2020**, *53*, 1351–1363. [CrossRef]
87. Shu, T.; Cossy, J. Enantioselective cross-couplings between halide derivatives and organometallics by using iron and cobalt catalysts.: Formation of C-C bonds. *Chem. Eur. J.* **2021**, *27*, 11021–11029. [CrossRef]
88. Liu, L.; Puga, A.V.; Cored, J.; Concepcion, P.; Pérez-Dieste, V.; García, H.; Corma, A. Sunlight-assisted hydrogenation of CO_2 into ethanol and C^{2+} hydrocarbons by sodium-promoted Co@ C nanocomposites. *Appl. Catal. B Environ.* **2018**, *235*, 186–196. [CrossRef]

89. Lebarbier, V.M.; Karim, A.M.; Engelhard, M.H.; Wu, Y.; Xu, B.Q.; Petersen, E.J.; Datye, A.K.; Wang, Y. The effect of zinc addition on the oxidation state of cobalt in Co/ZrO_2 catalysts. *Chemsuschem* **2011**, *4*, 1679–1684. [CrossRef]
90. Huang, Y.; Du, P.; Shi, W.-X.; Wang, Y.; Yao, S.; Zhang, Z.-M.; Lu, T.-B.; Lu, X. Filling COFs with bimetallic nanoclusters for CO_2-to-alcohols conversion with H_2O oxidation. *Appl. Catal. B Environ.* **2021**, *288*, 120001. [CrossRef]
91. Peng, T.; Wang, K.; He, S.; Chen, X.; Dai, W.; Fu, X. Photo-driven selective CO_2 reduction by H_2O into ethanol over $Pd/Mn\text{-}TiO_2$: Suitable synergistic effect between Pd and Mn sites. *Catal. Sci. Technol.* **2021**, *11*, 2261–2272. [CrossRef]
92. Liu, L.; Wang, S.; Huang, H.; Zhang, Y.; Ma, T. Surface sites engineering on semiconductors to boost photocatalytic CO_2 reduction. *Nano Energy* **2020**, *75*, 104959. [CrossRef]
93. Fan, Y.; Zhang, C.; Mamatkulov, S.; Ruzimuradov, O.; Low, J. Semiconductor facet junctions for photocatalytic CO2 reduction. *Pure Appl. Chem.* **2022**. [CrossRef]
94. Xiang, Y.; Cheng, B.-R.; Li, D.-F.; Zhou, B.-X.; Yang, T.-F.; Ding, S.-S.; Huang, G.-F.; Pan, A.; Huang, W.-Q. Facile one-step in-situ synthesis of type-II CeO_2/CeF_3 composite with tunable morphology and photocatalytic activity. *Ceram. Int.* **2016**, *42*, 16374–16381. [CrossRef]
95. Boltersdorf, J.; Forcherio, G.T.; McClure, J.P.; Baker, D.R.; Leff, A.C.; Lundgren, C. Visible light-promoted plasmon resonance to induce "hot" hole transfer and photothermal conversion for catalytic oxidation. *J. Phys. Chem. C* **2018**, *122*, 28934–28948. [CrossRef]